J Therm Anal Calorim (2012) 108:783–791
DOI 10.1007/s10973-011-2031-6

Characterization of the active sites in MgNiAl mixed oxides by microcalorimetry and test reaction

D. Meloni · M. F. Sini · M. G. Cutrufello · R. Monaci · E. Rombi · I. Ferino

MEDICTA2011 Conference Special Chapter

Abstract In this study, MgNiAl mixed oxides derived from layered double hydroxide precursors were prepared by pH-controlled co-precipitation. Three samples were prepared with a $(Mg^{2+} + Ni^{2+})/Al^{3+}$ ratio of 2 and a Ni^{2+}/Mg^{2+} with ratios of 0.22, 0.47, and 4.05. The structural, textural and redox features of the oxides were investigated by a variety of techniques, including X-ray diffraction, transmission electron microscopy, N_2 physisorption, and temperature-programmed reduction. The acid and base properties were assessed by NH_3 and CO_2 adsorption microcalorimetry, respectively. The acid–base features were also investigated by testing the catalytic behaviors of the oxides for the conversion of 4-methylpentan-2-ol under both mild and stressed conditions. The reactant alcohol can undergo dehydration into 4-methylpent-1-ene, 4-methylpent-2-ene, and skeletal isomers of C_6-alkenes, as well as dehydrogenation to 4-methylpentan-2-one and higher ketones, the product selectivity being governed by the concentration and strength of the acid and base sites. Comparison between the calorimetric and test reaction results is discussed.

Keywords MgNiAl mixed oxides · 4-Methylpentan-2-ol dehydration · Acidity/basicity · Microcalorimetry

D. Meloni (✉) · M. F. Sini · M. G. Cutrufello · R. Monaci · E. Rombi · I. Ferino
Dipartimento di Scienze Chimiche, Università di Cagliari, Complesso Universitario Monserrato, s.s. 554, Bivio Sestu, 09042 Monserrato, CA, Italy
e-mail: dmeloni@unica.it

Introduction

Hydrotalcites (LDHs) belong to the class of natural and synthetic anionic clays [1]. The hydrotalcite structure, with formula $Mg_6Al_2(OH)_{16}CO_3{\cdot}4H_2O$, resembles that of brucite, $Mg(OH)_2$. In brucite, magnesium cations are octahedrally coordinated by hydroxyl ions, giving rise to edge-shared layers of octahedra. In LDH materials, part of the Mg^{2+} ions are replaced by Al^{3+} ions, resulting in positively charged cation layers. Charge-balancing anions (usually CO_3^{2-}) and water molecules are situated in the interlayers between the stacked brucite-like cation layers [1, 2]. LDHs have attracted much attention in recent years as catalyst precursors. The thermal decomposition of these materials [3, 4] gives rise to mixed oxides composition and resistance to sintering of which make them interesting as industrial catalysts [1].

By the isomorphous substitution of Mg and Al cations of the LDHs with appropriate di- and trivalent cations, the acid–base properties of the ex-hydrotalcite oxides, as well as their redox properties, may be tailored, with the aim of obtaining bifunctional catalysts with a unique combination of such properties [5]. The basic character of ex-hydrotalcite oxides, usually assessed by temperature-programmed desorption (TPD) of carbon dioxide, is often invoked for explaining their catalytic activity in many reactions [6–8]. The drawback of such an approach is twofold: (i) it neglects any possible role of the acid sites, which might be simultaneously involved in the reaction mechanism; (ii) it relies on a technique which, though easy to use and straightforward to interpret on a qualitative basis, is unable to describe quantitatively the energetics of the interaction between the surface site and the probe molecule. Adsorption microcalorimetry is a direct, reliable technique for the investigation of the acid–base features of

solids [9–13]. By the simultaneous assessment of the adsorbed amount of a suitable probe molecule and the heat evolved at increasing coverage, the energetic features of surface sites can be pictured by processing the overall set of combined volumetric and calorimetric data. It is well known [14] that the catalytic conversion of alcohols is very sensitive to the acid–base properties of surfaces, and the conversions of propan-2-ol [15], butan-1-ol [16], and 2-methyl-3-butyn-2-ol [17] have been proposed as test reactions for the assessment of such features. In the case of propan-2-ol, the dehydration selectivity to propene and its dehydrogenation selectivity to acetone are directly traced back to the acidic and basic features, respectively, of the catalyst, but no information on the strength of the surface sites can be obtained. This point is addressed in [16], where the butan-1-ol dehydration to but-1-ene and dibutylether was correlated to the presence of acid sites of intermediate strength, whereas but-1-ene isomerization to *cis*-but-2-ene and *trans*-but-2-ene required strong and very strong acid sites. By using 2-methyl-3-butyn-2-ol the presence of acid sites (on which dehydration to 3-methyl-3-buten-1-yne and 3-methyl-2-buten-1-al occurs), basic sites (on which decomposition to acetone and acetylene takes place), and acid–base pairs (which catalyze 3-methyl-3-buten-2-one and 3-hydroxy-3-methyl-2-butanone formation) can be revealed, but the strenght of the sites remains unexplored. In comparison, the use of 4-metylpentan-2-ol as the reactant alcohol seems to be able to provide a wealth of information, because both the number and strength of the acid and base sites are responsible for the possible occurrences of (i) two competing reactions, namely, dehydration to the corresponding 1- and 2-alkenes and dehydrogenation to 4-methylpentan-2-one, (ii) three different reaction mechanisms for the dehydration reaction, namely E1, E2, and E1cB, (iii) consecutive isomerization and condensation reactions involving the alkenes and the ketones, respectively. The conversion of 4-metylpentan-2-ol has been widely investigated in the present authors' laboratory [18–29] with the practical aim of screening active and selective catalysts for the transformation of 4-metylpentan-2-ol into 4-methylpent-1-ene, starting material for the manufacture of polymers of superior technological properties. It was found by adsorption microcalorimetry of ammonia and CO_2 that the selectivity to the diverse products can be governed by the fine tuning of the number and strength of the acid and base sites. Based on this, monitoring of the products distribution of the 4-methylpentan-2-ol transformation seems a useful tool for determining the acid–base properties of solids. This method has been used, in association with adsorption microcalorimetry, for the study of diverse oxides [30] and, more recently, for the investigation of LDH-derived materials [31, 32].

The present article is a further contribution to the characterization of ex-hydrotalcite mixed oxides by the combined use of adsorption microcalorimetry and 4-methylpentan-2-ol reaction. Three hydrotalcite samples were prepared by pH-controlled co-precipitation with a $(Mg^{2+} + Ni^{2+})/Al^{3+}$ ratio of 2 and a Ni^{2+}/Mg^{2+} ratios of 0.22, 0.47, and 4.05. The LDH materials were characterized by X-ray diffraction (XRD) and transmission electron microscoy (TEM), to check their structural features. Through a calcination step, the hydrotalcite samples were converted into mixed oxides, which, after XRD and nitrogen physisorption characterization, were studied by ammonia and carbon dioxide adsorption microcalorimetry, as well as by catalytic testing for 4-methylpentan-2-ol conversion in long-lasting runs under both mild and stressed conditions. Perturbation of the products distribution should be expected if the redox features of the catalyst, possibly stemming from the presence of Ni in the mixed oxides, were also involved in the 4-methylpentan-2-ol conversion. Actually, the conversion of alcohols into carbonyl compounds, such as aldehydes [33] and ketones [34] at low temperatures, has been reported in the case of Cu-based catalysts. To address this point, the redox properties of the LDH-derived mixed oxides were also investigated by the temperature-programmed reduction (TPR) technique.

Experimental

Materials

4-Methylpentan-2-ol (analytical grade) and nitric acid (HNO_3, 63%) were provided by Fluka. Magnesium nitrate ($Mg(NO_3)_2{\cdot}6H_2O$), nickel nitrate ($Ni(NO_3){\cdot}6H_2O$), aluminum nitrate ($Al(NO_3)_3{\cdot}9H_2O$), potassium carbonate (99.99%), and sodium hydroxide (analytic grade) were supplied by Sigma-Aldrich. Ammonia (99.9%) and carbon dioxide (99.9%) were purchased from Air Liquide.

LDHs and mixed oxides preparation

The LDH precursors with different Mg/Ni/Al molar ratios were prepared by pH-controlled co-precipitation, under low supersaturation, of the corresponding metal nitrate salts. The synthesis was carried out keeping constant the M^{2+}/M^{3+} ratio equal to 2 (where $M^{2+} = Mg^{2+}$, Ni^{2+}, and $M^{3+} = Al^{3+}$), while the relative proportions of Mg and Ni were variable. In a typical synthesis, an aqueous solution of the metal nitrates with a total cation concentration of 1.5 M and an aqueous basic solution (used as a pH controlling agent), containing 0.8 M of Na_2CO_3 and 1.6 M of NaOH, were simultaneously introduced by two dosing pumps in a flask fitted with a pH electrode and containing a small

amount of deionized water. The suspension was vigorously stirred at 308 K and maintained at constant pH of 9 by adjusting the relative flow rates of the two solutions. After complete addition of the metal salts, the final suspension was aged under stirring at 308 K for 16 h. The resulting solid was recovered by filtration, washed with deionized water, and dried overnight at 313 K. Three samples were prepared and labeled as LDH(0.22), LDH(0.47), and LDH(4.05), where the figures within parenthesis indicate the Ni^{2+}/Mg^{2+} molar ratio. The corresponding mixed oxides, denoted as MgNiAl(0.22), MgNiAl(0.47), and MgNiAl(4.05), were obtained from the LDH samples by calcination in oven at 723 K for 6 h (heating rate 3 K min^{-1}).

Characterization techniques

The Mg, Ni, and Al contents were determined by inductively coupled plasma atomic emission spectrometry (ICP-AES) analysis by using a LIBERTY 200–VARIAN instrument. Samples (50 mg) were treated with 10 cm^3 of a nitric acid solution (1 M) at room temperature and diluted to 250 cm^3.

XRD patterns were recorded with a 0.100° step on a Seifert diffractometer using Cu-Kα radiation ($\lambda = 1.5406$ Å).

TEM images were obtained on a JEOL 200 CX microscope equipped with a tungsten cathod operating at 200 kV. The sample was dispersed in *n*-octane by sonication, dropped on a carbon-coated copper grid and dried for observation.

Textural analyses were performed using a Thermofinnigan Sorptomatic 1990 apparatus by determing the nitrogen adsorption/desorption isotherms at 77 K. Before the analysis, the samples were pretreated overnight at 673 K under vacuum (10^{-3} Pa). Specific surface areas and pore volumes were determined by the BET method. Pore–size distribution plots were obtained from the desorption branch of each isotherm by the BJH method.

Temperature-programmed reduction (TPR) analysis was carried out in a Prolab TPD/R/O 1100 instrument. After activation of the sample (50 mg) under air (15 cm^3 min^{-1}) at 723 K (10 K min^{-1}) for 6 h and cooling to room temperature, TPR runs were performed between 303 and 1073 K (20 K min^{-1}) in a stream of 5 vol% H_2 in N_2 (30 cm^3 min^{-1}). The H_2 consumption was evaluated by monitoring the flowing carrier gas through a hot-wire detector (HWD). A 3A molecular sieve trap was used to remove water.

A Tian-Calvet heat flow calorimeter (Setaram) equipped with a volumetric vacuum line was used for microcalorimetric measurements. After calcination in air at 723 K for 6 h, each sample (100 mg) was pre-treated overnight at 673 K under vacuum (10^{-3} Pa) before adsorption. Adsorption was carried out at 353 K by admitting successive doses of probe molecule (ammonia or carbon dioxide) and recording the thermal effect. The run was stopped at a final pressure of 133.3 Pa.

Catalytic runs

4-Methylpentan-2-ol conversion was carried out at atmospheric pressure in a fixed-bed flow microreactor. To avoid thermal conversion of the reactant, a quartz microreactor was used, and all the stainless steel lines to and from the reactor were passivated by immersion of pipes into hot diluted HNO_3 for 2 h, followed by thorough washing and drying, before assembling the catalytic equipment. Test runs were also performed in the empty reactor, showing a conversion below 0.5%. After activation in situ (12 h at 723 K under CO_2-free air flow), 4-methylpentan-2-ol was fed into the reactor (mass of catalyst, $m_{cat} = 0.1$ g) with an N_2 stream (alcohol partial pressure, $p_{o,\ alcool} = 18.4$ kPa). The reaction was carried out for 8 h under both mild (473 K and contact time, $\tau = 0.01$ g_{cat} h $g_{alcohol}^{-1}$) and stressed conditions (623 K, contact time, $\tau = 0.52$ g_{cat} h $g_{alcohol}^{-1}$).

The reaction mixture was analyzed by online gas chromatography using a fused silica capillary column (Petrocol from Supelco, 50 m length, 0.20 mm i.d., 0.50 μm film thickness). Product separation was carried out using the following analysis program: $T_{initial} = 323$ K for 15 min, heating rate 10 K min^{-1}, $T_{final} = 473$ K for 10 min. The identification of the reaction products (4-methylpent-1-ene (1-Alk), 4-methylpent-2-ene, *cis* and *trans* (2-Alk), skeletal isomers of C_6-alkenes (i-C_6), 4-methylpentan-2-one (K), and heavy ketones (HK)) was checked by GC/MS.

Results and discussion

Structural and textural characterization of LDHs and MgNiAl mixed oxides

The XRD patterns of the LDH samples (not shown for brevity) were typical of the hydrotalcite structure, with intense sharp and symmetric peaks at $2\theta = 11.55°$ (hkl: 003), 23.35° (hkl: 006), 60.23° (hkl: 110) and 61.55° (hkl: 113), and broad and asymmetric peaks at $2\theta = 34.57°$ (hkl: 102), 39.17° (hkl: 105) and 46.77° (hkl: 108) [31]. No excess phase was detected, suggesting that the Ni^{2+} cations have isomorphously substituted the Mg cations in the hydrotalcite structure [31, 35]. From the position of the most intense peaks with crystallographic indices (003) and (110), the lattice distances d_{003} and d_{110} can be used to calculate the two lattice parameters *a* and *c*, where

a ($2 \times d_{110}$) corresponds to the cation–cation distance within the brucite-like layer, while c ($3 \times d_{003}$) is related to the total thickness of the brucite-like layer and the interlayer distance. The value of parameter a is very sensitive to the nature (ionic radii) of the layer cations, while the value of parameter c strongly depends on the nature and orientation of the interlayer anion. For the present samples, the calculated a and c values are: 3.012 and 22.162 Å for LDH(0.22); 3.039 and 22.046 Å for LDH(0.47); 3.051 and 22.918 Å for LDH(4.05). These values are close to those reported in the literature for this type of material [6, 31]. Expectedly, the parameter a increases with the degree of substitution of Mg^{2+} ions (ionic radius 0.65 Å) by Ni^{2+} ions (ionic radius 0.69 Å). Since there is the same anion (carbonate) for all the LDH samples, the variations observed in the c parameter can be ascribed, as suggested in the literature [35], to differences in the hydratation extent.

TEM images for the LDH(4.05) sample are shown in Fig. 1. The characteristic filament-like morphology of the hydrotalcite materials is clearly visible (Fig. 1a), with filament lengths up to 200 nm. At higher magnification, in the dark field mode (Fig. 1b), the material appears composed of very small crystals (ca. 3 nm). The electron diffraction pattern (Fig. 1c) confirms the hydrotalcite phase.

The typical reflections of the hydrotalcite structure were no longer visible in the XRD patterns of the materials obtained upon calcining the LDH samples at 723 K (not shown). Broad peaks were visible at 63.2, 43.6, and 36.1° for MgNiAl(0.22); 63.2, 43.5, and 36.3° for MgNiAl(0.47); 63.5, 43.8, and 37.3° for MgNiAl(4.05). Based on the PDF cards for MgO(78-0430) and NiO(45-0946), and taking into account the composition of the samples, the patterns for the low-Ni content samples could be reasonably assigned to a poorly crystallized MgO-dominated cubic phase, whereas the reflections in the MgNiAl(4.05) pattern, which appear slightly shifted toward higher angles, could be assigned to a poorly crystallized NiO-dominated cubic phase.

The nitrogen adsorption–desorption isotherms of the mixed oxides (not shown for brevity) were of type IV (IUPAC classification [36]), characteristic of mesoporous solids, with a H3-type hysteresis loop, which is typical of slit-shaped pores. The calculated values of BET surface area and pore volume were 154 $m^2\ g^{-1}$ and 0.38 $cm^3\ g^{-1}$ for MgNiAl(0.22); 359 $m^2\ g^{-1}$ and 0.67 $cm^3\ g^{-1}$ for MgNiAl(0.47); 282 $m^2\ g^{-1}$ and 0.54 $cm^3\ g^{-1}$ for MgNiAl (4.05). Pore-size distribution plots (not shown) exhibited an unimodal pore distribution centered at 3.8 nm.

The TPR profile of MgNiAl(4.05) is reported in Fig. 2. It shows a sharp peak at 713 K, which merges into a very large one centered around 823 K. The only reducible species present in the sample is Ni^{2+}, so that the hydrogen consumption during the run is related to its transformation into Ni metal. The TPR profile hence suggests that Ni^{2+} is present in the sample in (at least) two different environments. The detailed discussion of the this point is, however, beyond the scope of the present study. The aim of the TPR runs was to check whether the redox features of the oxides could play some role in the catalysis of 4-methylpentan-2-ol conversion. As the reduction of the Ni^{2+} species sets in well above the highest temperature used for catalytic testing (623 K), any contribution from a redox mechanism to the catalytic activity can be ruled out.

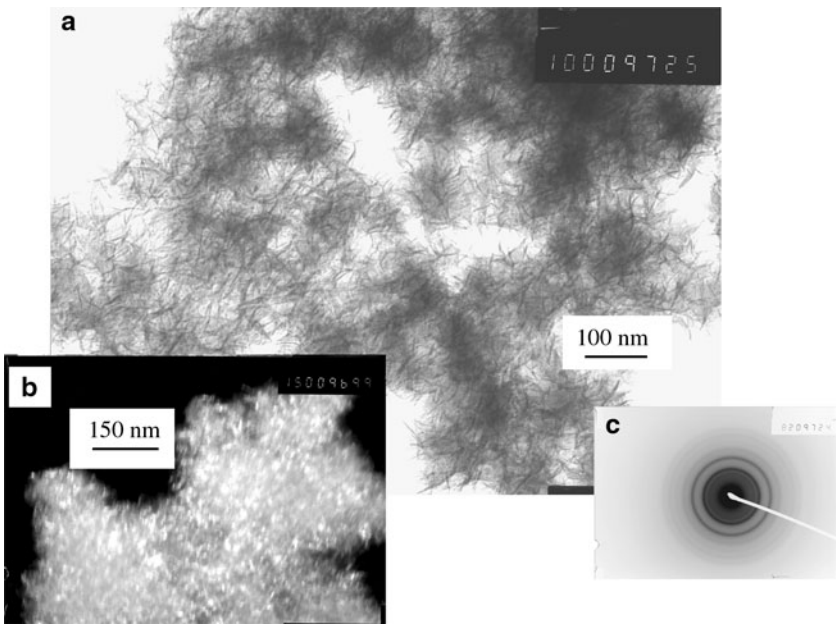

Fig. 1 TEM images for LDH(4.05) hydrotalcite: bright field mode (**a**), dark field mode (**b**), and electron diffraction pattern (**c**)

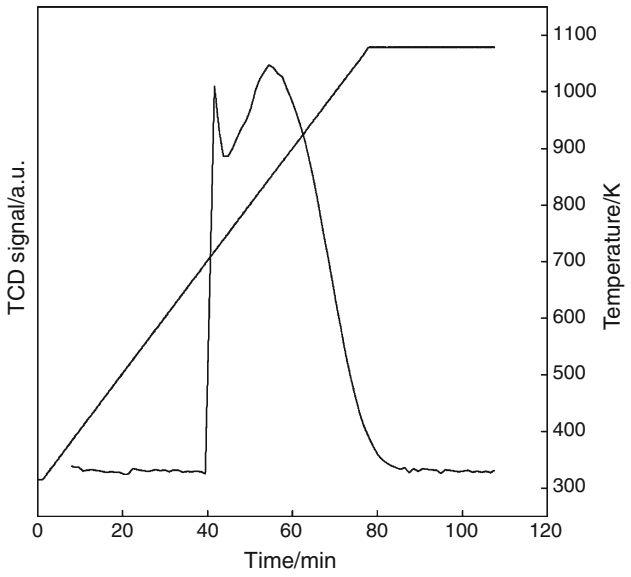

Fig. 2 TPR profile for LDH(4.05) hydrotalcite

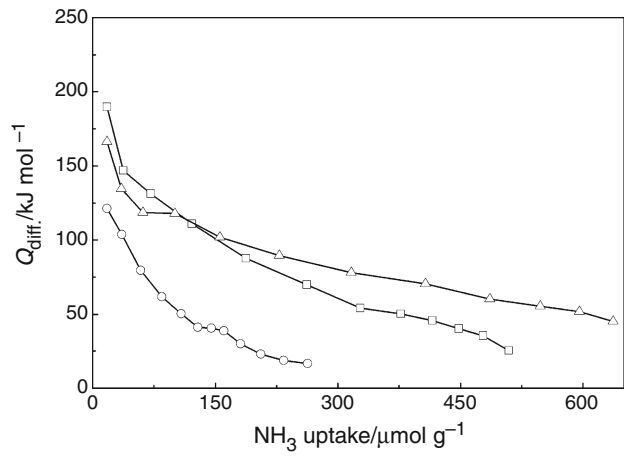

Fig. 3 Differential heat versus uptake for ammonia adsorption at 353 K for the MgNiAl(0.22) (*open circle*), MgNiAl(0.47) (*open triangle*), and MgNiAl(4.05) (*open square*) mixed oxides

Microcalorimetric investigation of the mixed oxides

The calorimetric results for all the samples are summarized in Figs. 3, 4, 5, and 6 for NH_3 and CO_2 adsorption. The differential heat of adsorption, Q_{diff}, is plotted versus the ammonia uptake in Fig. 3. The initial Q_{diff} values are 189, 166, and 121 kJ mol^{-1} for MgNiAl(4.05), MgNiAl(0.47), and MgNiAl(0.22), respectively, which reveals the presence of strong acid sites. For all the samples, the differential heat decreases as the ammonia uptake increases, thus indicating heterogeneity of the sites. At high coverage values, physisorption can take place, and its contribution to the ammonia uptake should be neglected in the assessment of the acid site concentration, n_A. Typically, the heat released during physisorption is twice as large as the condensation heat [37], which, in the case of ammonia at 353 K is 20.2 kJ mol^{-1} [38]. Accordingly, the fraction of ammonia uptake in Fig. 3 corresponding to differential heats below 40 kJ mol^{-1} was ascribed to physical adsorption and was neglected in calculating the acid site concentration. The obtained n_A values are 448, 637, and 146 μmol g^{-1} for MgNiAl(4.05), MgNiAl(0.47), and MgNiAl(0.22), respectively.

The Q_{diff} versus ammonia uptake profiles can be used to obtain the site-energy distribution plots. These are shown in Fig. 4, where the negative inverse of the first derivative of the differential heat with respect to n_A ($-dn_A/dQ_{diff}$) is plotted versus n_A for the mixed oxide samples. The apperance of peaks in the site-energy distribution plots reveals that sets of homogenous sites, i.e., interacting with the probe with similar strength, are present on the surface. The higher the area under the peak, the higher the population of the corresponding family of sites. Accordingly,

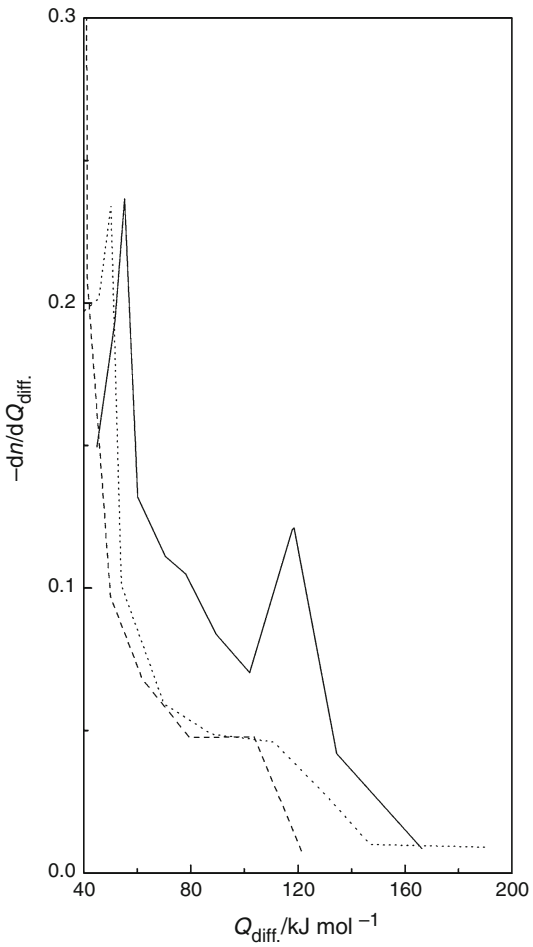

Fig. 4 Site-energy distribution plots for MgNiAl(0.22) (*dashed line*), MgNiAl(0.47) (*straight line*), and MgNiAl(4.05) (*dotted line*) mixed oxides, as obtained through graphical derivation curves of Fig. 3

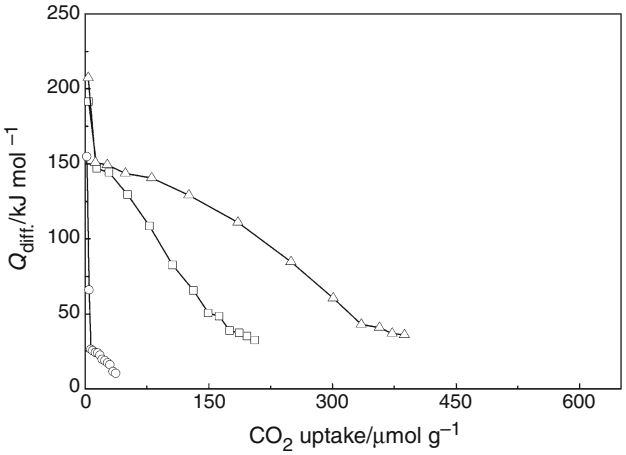

Fig. 5 Differential heat versus uptake for carbon dioxide adsorption at 353 K for the MgNiAl(0.22) (*open circle*), MgNiAl(0.47) (*open triangle*), and MgNiAl(4.05) (*open square*) mixed oxides

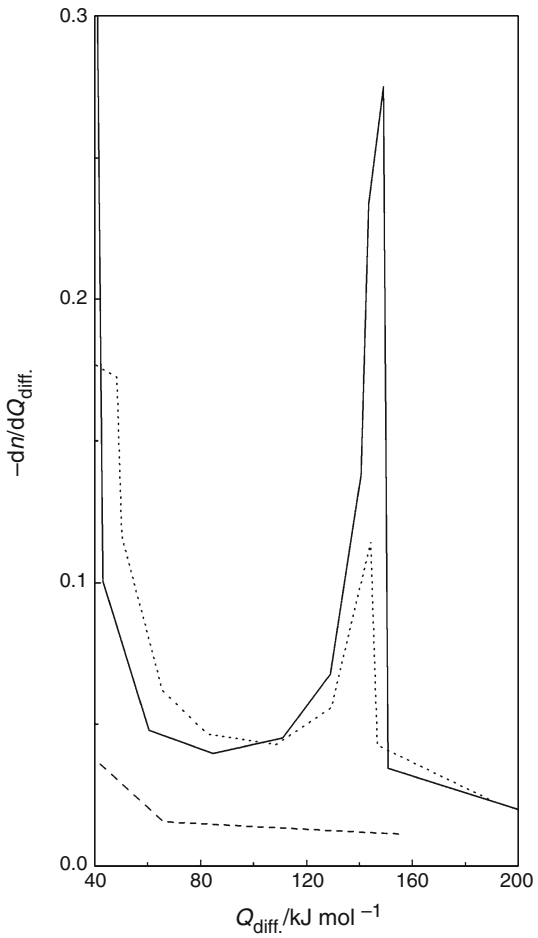

Fig. 6 Site-energy distribution plots for MgNiAl(0.22) (*dashed line*), MgNiAl(0.47) (*straight line*), and MgNiAl(4.05) (*dotted line*) mixed oxides, as obtained through graphical derivation curves of Fig. 5

the two peaks visible in the plot for MgNiAl(0.47) correspond to two sets of homogeneous sites, whose strength of which is around 55 and 120 kJ mol^{-1}, respectively. One family of homogeneous sites is present on MgNiAl(4.05) (peak at 50 kJ mol^{-1}). The lack of peaks in the site-energy distribution plot for MgNiAl(0.22) indicates continuous heterogeneity of the sites on this sample.

The differential heat for CO_2 adsorption is plotted versus the uptake in Fig. 5. Strong basic sites are present on all the samples, as indicated by the initial Q_{diff} values: 191, 207, and 154 kJ mol^{-1} for MgNiAl(4.05), MgNiAl(0.47), and MgNiAl(0.22), respectively. Heterogeneity of the samples is revealed by the decreasing trend of Q_{diff} with increasing the CO_2 uptake. The concentrations of basic sites, n_B, are calculated from the total CO_2 uptake by neglecting the fraction corresponding to differential heats below 27 kJ mol^{-1} (twice the condensation heat of CO_2 at 353 K [37]) are 206, 388, and 7 μmol g^{-1} for MgNiAl (4.05), MgNiAl(0.47), and MgNiAl(0.22), respectively. The site-energy distribution plot for carbon dioxide adsorption is shown in Fig. 6. A large peak, centered at 150 kJ mol^{-1}, is visible in the plot for MgNiAl(0.47), which points out to the presence of a large set of homogeneous, strong basic sites. The same family of sites is also present on the surface of MgNiAl(4.05), but its population is remarkably lower. Continuous heterogeneity of the sites is observed on MgNiAl(0.22).

4-Methylpentan-2-ol conversion

The transformation of 4-methylpentan-2-ol to the mixed oxides under mild conditions ($T = 473$ K and $\tau = 0.01$ g_{cat} h $g^{-1}_{alcohol}$) gave only dehydration products, namely, 4-methylpent-1-ene (1-Alk), *cis* and *trans* 4-methylpent-2-ene (2-Alk), skeletal isomers of C_6-alkenes (i-C_6). The conversion level was about 23 mol% for all the samples, and no catalyst aging was observed over 8 h on-stream. The selectivity results showed that, whatever the sample, skeletal isomers of C_6-alkenes (68–65 mol%) and 4-methylpent-2-ene (27–23 mol%) were by far predominant over 4-methylpent-1-ene (9–7 mol%).

The first step of secondary alcohol transformation over metal oxide catalysts is the adsorption of the reactant on the surface. The adsorbed alcohol species can be converted through a two-step mechanism involving intermediate carbocation formation (E1), a concerted pathway (E2) or through carbanion formation mechanism (E1cB) [14]. These mechanisms should be regarded as limiting cases, since intermediate situations can occur. In the E1 mechanism, Saytzeff orientation, leading to alkenes with the double bond in internal position, is expected. Also in the E2 mechanism Saytzeff products would prevail over the alkene with the double bond in terminal position. By

converse, the E1cB mechanism would lead to the Hofmann product, i.e., the 1-alkene. Both the E1cB and E2 mechanisms would require a balanced number of basic and acid sites, in order that a two-point adsorption of the reactant alcol can set in through the interaction of a basic site with the H atom of the methyl group and of an acid site with the O atom of the hydroxy group. If the strength of the basic sites is higher than that of the acid ones, then the E1cB mechanism, i.e., the rupture of the C–H bond first, followed by carbanion formation and OH release to give the 1-alkene, should occur. If the basic and acid sites are of comparable strength, then the E2 mechanism, i.e., the simultaneous breaking of the C–H and C–OH bonds, would take place, leading to the 2-alkene. When the the acid site concentration is high compared to that of the basic sites, the E1 mechanism occurs: it is initiated by the attack of an acid site on the OH group of the reactant alcohol, followed by the formation of a carbocation, which releases a proton to give the corresponding alkene with internal double bond. If strong acid sites are present, then skeletal isomers of C_6-alkenes should also be formed, owing to alkyl shift in the carbocation.

The formation of the Saytzeff product, which undergoes consecutive isomerization to a remarkable extent, suggests that the E1 mechanism is operating on the MgNiAl mixed oxides, which in turn indicates that (i) the acid sites prevail on the basic ones, and (ii) acid sites strong enough to isomerize the 2-alkene are present. It is worthy to note that the possible occurrence of the E2 mechanism can be ruled out on the basis of calorimetric data: the calculated values of the n_B:n_A ratio are 0.05, 0.61, and 0.46 for MgNiAl(0.22), MgNiAl(0.47), and MgNiAl(4.05), respectively, which means that the concentrations of basic and acid sites are so imbalanced that the two-point adsorption cannot set in. For the same reason, also the establishing of the E1cB mechanism is hindered, which is in agreement with the observed very low selectivity to the Hofmann product. It is also interesting to note that the fraction of acid sites stronger than 80 kJ mol^{-1} (reasons for such limit stem from previous findings [18–29]), $n_{A>80}$:n_A, is 0.40 for MgNiAl(0.22), 0.47 for NiMgAl(0.47), and 0.50 for NiAlMg(4.05), which is consistent with the occurrence of the 2-alkene isomerization.

The 4-methylpentan-2-ol conversion over the mixed oxides under stressed conditions ($T = 623$ K and $\tau = 0.52$ g_{cat} h $g^{-1}_{alcohol}$) gave dehydration products as well as dehydrogenation products, namely, 4-methylpentan-2-one (K) and heavy ketones (HK). The initial conversion was ca. 95 mol% for NiMgAl(0.22), with a decrease to ca. 80 mol% after 8 h on-stream, and ca. 100 mol% for both NiMgAl(0.47) and NiMgAl(4.05); a decrease to ca. 95 mol% was observed on the former, whereas no significant deactivation was observed on the latter. The selectivity trends with time-on-stream are shown in Fig. 7. Remarkable differences can be observed between NiMgAl(0.22) on the one side and NiMgAl(0.47) and NiMgAl(4.05) on the other. Dehydration is the main reaction occurring on NiMgAl(0.22), the highest selectivity being that to 2-alkene (41-44 mol%, over 8 h on-stream), followed by that to 1-alkene (20–22 mol%), and that to i-C_6 (18–19 mol%). Dehydrogenation to 4-methylpentan-2-one also occurred to some extent (ketone selectivity = 15–20 mol%). By converse, the selectivity to dehydration products is negligible on MgNiAl(0.47): it can be regarded as a powerful dehydrogenation catalyst, over which the primary product (4-methylpentan-2-one) undergoes condensation reactions leading to higher ketones (HK). Such secondary reactions are by far predominant during the first period on-stream (S_{HK} = 94–87 mol%); from the third hour onward, *and* S_{HK} starts decreasing and 4-methylpentan-2-one tends to become the major product. Also MgNiAl(4.05) is virtually a dehydrogenation catalyst, the selectivity to the dehydration products (1-Alk, 2-Alk and i-C_6) being very low. At variance with the case of

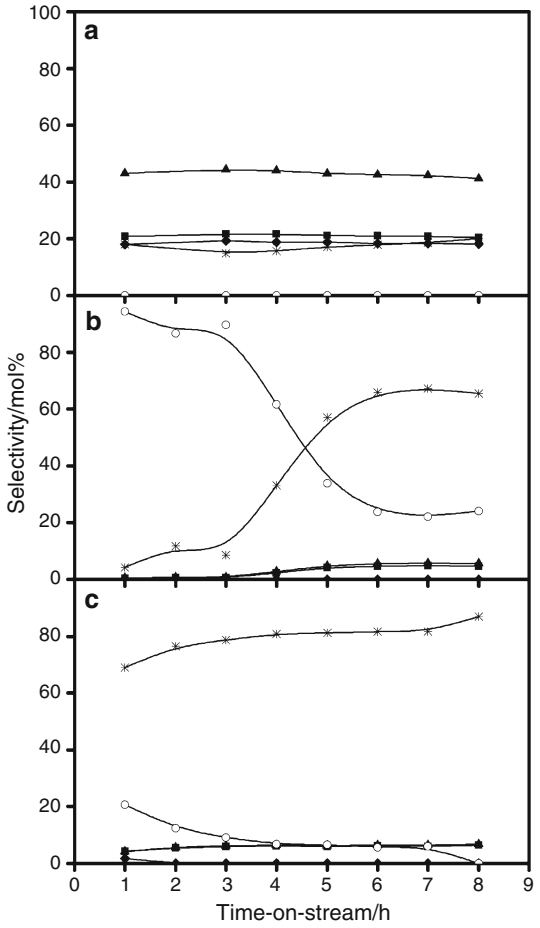

Fig. 7 Selectivities to 1-Alk (*filled square*), 2-Alk (*filled triangle*), i-C_6 (*filled diamond*), K (*asterisk*), and HK (*open circle*) products versus time-on-stream for MgNiAl(0.22) (**a**), MgNiAl(0.47) (**b**), and MgNiAl(4.05) (**c**) mixed oxides, at 623 K and $\tau = 0.52$ g g^{-1} h^{-1}

MgNiAl(0.47), the extent of consecutive reactions involving the primary ketone is low, and the influence of time-on-stream on S_K and S_{HK} rather limited.

It is generally assumed [14] that when the E1cB mechanism is operating, there is a tendency for dehydrogenation to occur to some extent: the ketone formation would stem from the elimination of a hydride ion (instead of OH^-) from the carbanionic species. For catalysts with a concentration of the basic sites higher than that of the acid ones, the E1cB mechanism is unlikely, and dehydrogenation can occur through another mechanism, as suggested in [39, 40] on the basis of quantum chemical calculation and confirmed for a variety of metal oxides in [30]. In this mechanism, the reactant alcohol is adsorbed on the basic sites by means of a hydrogen bond, the C_α–O bond being strengthened and the C_α–H bond weakened by localization of the negative charge on H_α; C_α–H bond rupture can then occur, the H_α being abstracted by interaction with a positively polarized H atom of the surface (originating from the previously split O–H group of the alcohol). A key requirement is that the basic sites strength is high enough.

From the selectivity values to the different alkenes (Fig. 7), it is apparent that neither the E1 nor the E2 and E1cB mechanisms take place to a significant extent on MgNiAl(0.47) and MgNiAl(4.05). This leads us to conclude that for these oxides (i) the concentration of the basic sites prevails over that of the acid sites, and (ii) the strength of the basic sites is high. The basic function seems particularly high for MgNiAl(0.47), as suggested by the remarkable occurrence of basic-catalyzed condensation reactions leading to higher ketones. The decrease of S_{HK} with time-on-stream observed for this oxide is reasonably related to the deactivation of the stronger sites, on which the condensation products remain strongly adsorbed. At first sight, the above-outlined conclusions, drawn from the catalytic runs under stressed conditions, seem to be at variance with the calorimetric results, which indicate that acid sites prevail over the basic ones (n_B:n_A ratios = 0.61 and 0.46 for MgNiAl(0.47) and MgNiAl(4.05), respectively). It could be reasoned, however, that at the high reaction temperature of the catalytic run, only the stronger sites would be involved in the reaction, the weak ones being unable to significantly interact with the reactant alcohol. Though no detailed discussion can be attempted, a clue to which sites might participate in the reaction can be obtained from the site-energy distribution plots. A large family of strong basic sites (Q_{diff} in the range 110–150 kJ mol^{-1}) is present on MgNiAl(0.47) (Fig. 6); in this same region of strength, a family of acid sites is also present on such oxide (Fig. 4). Assuming that only these two sets of sites are strong enough to be involved in the reaction at 623 K, the ratio between the basic and acid sites, $n_{B(110–150)}$:$n_{A(110–150)}$, should measure the relative amounts of basic and acid sites, rather than the n_B:n_A ratio. For MgNiAl(0.47), the calculated value of the $n_{B(110–150)}$:$n_{A(110–150)}$ ratio is 2.0, i.e., among the sites that are able to interact with the reactant alcohol, the basic sites are by far the most abundant, which is consistent with the outcome of the catalytic runs. The same holds for MgNiAl(4.05), for which the $n_{B(110–150)}$:$n_{A(110-150)}$ ratio is 1.4. By converse, in the case of MgNiAl(0.22), the acid sites are the most abundant among the sites that are able to interact with the reactant alcohol at high temperature ($n_{B(110–150)}$:$n_{A(110–150)}$ = 0.6), which is consistent with the observed predominance of dehydration over dehydrogenation over this oxide.

Conclusions

MgNiAl hydrotalcite materials, synthesized with a $(Ni^{2+} + Mg^{2+})/Al^{3+}$ ratio of 2 and Ni^{2+}/Mg^{2+} ratios of 0.22, 0.47, and 4.05, thermally decompose at 723 K to yield the corresponding mixed oxides, NiMgAl(x), where $x = Ni^{2+}/Mg^{2+}$ ratio. Such oxides have acid, basic, and redox properties.

There is no contribution of the redox properties to the catalytic activity of the oxides for the 4 methylpentan-2-ol at both 473 and 623 K, due to the high (>673 K) Ni^{2+}/Ni^0 reduction temperature.

On the surface of all the oxides, the acid sites are exposed at a higher concentration than the basic ones, as indicated by both catalytic testing at 473 K (no dehydrogenation activity observed, with E1 mechanism for dehydration operating) and adsorption microcalorimetry (ratio between the concentration of the CO_2-interacting sites and the concentration of the ammonia-interacting sites at 353 K in the range 0.05–0.61).

At 623 K NiMgAl(0.47) and NiAlMg(4.05) behave as dehydrogenating catalysts, as a consequence of the involvement of strong basic sites in the reaction. The 4-methylpentan-2-ol conversion is mostly dehydration-oriented on MgNiAl(0.22), on which the reaction is governed by acid sites (E1 mechanism). Not all the sites titrated by ammonia and carbon dioxide in calorimetric experiments at 353 K are able to interact with the reactant alcohol at a temperature as high as 623 K. It is tentatively proposed that the active sites are those of basic and acid strengths in the 110–150 kJ mol^{-1} range.

References

1. Cavani F, Trifirò F, Vaccari A. Hydrotalcite-type anionic clays: preparation, properties and applications. Catal Today. 1991;11:173–301.
2. Van der Pol A, Mojet BL, Van der Ven E, De Boer E. Ordering of intercalated water and carbonate anions in hydrotalcite. An NMR study. J Phys Chem. 1994;98:4050–4.

3. Queiroz RM, Pires LHO, de Souza RCP, Zamian JR, de Souza AG, da Rocha Filho GN, da Costa CEF. Thermal characterization of hydrotalcite used in the transesterification of soybean oil. J Therm Anal Calorim. 2009;97:163–6.
4. Palmer SJ, Spratt HJ, Frost RL. Thermal decomposition of hydrotalcites with variable cationic ratios. J Therm Anal Calorim. 2009;95:123–9.
5. Vaccari A. Clays and catalysis: a promising future. Appl Clay Sci. 1999;14:161–98.
6. Valente JS, Hernandez-Cortez J, Cantu MS, Ferrat G, López-Salinas E. Calcined layered double hydroxides Mg–Me–Al (Me: Cu, Fe, Ni, Zn) as bifunctional catalysts. Catal Today. 2010;150:340–5.
7. McKenzie AL, Fishel CT, Davis RJ. Investigation of the surface structure and basic properties of calcined hydrotalcites. J Catal. 1992;138:547–61.
8. Kuśtrowski P, Chmielarz L, Bożek E, Sawalha M, Roessner F. Acidity and basicity of hydrotalcite derived mixed Mg–Al oxides studied by test reaction of MBOH conversion and temperature programmed desorption of NH_3 and CO_2. Mater Res Bull. 2004;39:263–81.
9. Gravelle PC. Heat-flow microcalorimetry and its application to heterogeneous catalysis. Adv Catal. 1972;2:191–263.
10. Auroux A. Les techniques Physiques d'Étude des Catalyseurs. In: Imelik B, Védrine JC, editors. Les techniques physiques d'étude des catalyseurs. Ch. 24. Paris: Editions Technip; 1988. p. 823.
11. Cardona-Martinez N, Dumesic JA. Applications of adsorption microcalorimetry to the study of heterogeneous catalysis. Adv Catal. 1992;38:149–244.
12. Andersen PJ, Kung HH. Catalysis, specialist periodical reports. In: Bond GC, Webb G, editors. Ch. 11. London: The Royal Society of Chemistry; 1994.
13. Solinas V, Ferino I. Microcalorimetric characterization of acid-basic catalysts. Catal Today. 1998;41:179–89.
14. Winterbottom JM. Hydration and dehydration by heterogeneous catalysts. In: Kemball C, Dowden DA, editors. Catal R Soc Chem 1981;4:141–74.
15. Gervasini A, Auroux A. Acidity and basicity of metal oxide surfaces II. Determination by catalytic decomposition of isopropanol. J Catal. 1991;131:190–8.
16. Berteau P, Delmon B, Dallons JL, Van Gysel A. Acid-base properties of silica-aluminas: use of 1-butanol dehydration as a test reaction. Appl Catal. 1991;70:307–23.
17. Lauron-Pernot H, Luck F, Popa JM. Methylbutynol: a new and simple diagnostic tool for acidic and basic sites of solids. Appl Catal. 1991;78:213–25.
18. Auroux A, Artizzu P, Ferino I, Solinas V, Leofanti G, Padovan M, Messina G, Mansani R. Dehydration of 4-methylpentan-2-ol over zirconia catalysts. J Chem Soc Faraday Trans. 1995;91:3263–7.
19. Auroux A, Artizzu P, Ferino I, Monaci R, Rombi E, Solinas V, Petrini G. Dehydration of 4-methylpentan-2-ol over lanthanum and cerium oxides. J Chem Soc Faraday Trans. 1996;92:2619–24.
20. Auroux A, Artizzu P, Ferino I, Monaci R, Rombi E, Solinas V. Conversion of 4-methylpentan-2-ol over alkali–metal ion-exchanged X and Y zeolites: a microcalorimetric and catalytic investigation. Micropor Mater. 1997;11:117–26.
21. Cutrufello MG, Ferino I, Solinas V, Primavera A, Trovarelli A, Auroux A, Picciau C. Acid-base properties and catalytic activity of nanophase ceria-zirconia catalysts for 4-methylpentan-2-ol dehydration. Phys Chem Chem Phys. 1999;1:3369–75.
22. Ferino I, Casula MF, Corrias A, Cutrufello MG, Monaci R, Paschina G. 4-Methylpentan-2-ol dehydration over zirconia catalysts prepared by sol-gel. Phys Chem Chem Phys. 2000;2:1847–54.
23. Colón G, Navío JA, Monaci R, Ferino I. CeO_2–La_2O_3 catalytic system. Part I. Preparation and characterisation of catalysts. Phys Chem Chem Phys. 2000;2:4453–9.
24. Mulas G, Monagheddu M, Cocco G, Cutrufello MG, Ferino I, Rombi E. Conversion of 4-methylpentan-2-ol over powder catalysts prepared by ball milling. J Mater Synth Process. 2000;8:385–91.
25. Cutrufello MG, Ferino I, Monaci R, Rombi E, Colón G, Navío JA. CeO_2–La_2O_3 catalytic system. Part II. Acid–base properties and catalytic activity for 4-methylpentan-2-ol dehydration. Phys Chem Chem Phys. 2001;3:2928–34.
26. Cutrufello MG, Ferino I, Monaci R, Rombi E, Solinas V. Doped zirconia catalysts for the dehydration of 4-methylpentan-2-ol. Stud Surf Sci Catal. 2001;140:175–84.
27. Solinas V, Rombi E, Ferino I, Cutrufello MG, Colón G, Navío JA. Preparation, characterisation and activity of CeO_2–ZrO_2 catalysts for alcohol dehydration. J Mol Catal A Chem. 2003;204–205:629–35.
28. Cutrufello MG, Ferino I, Rombi E, Solinas V, Colón G, Navío JA. Catalytic activity of Ceria-Lanthana system for 4-methylpentan-2-ol dehydration. React Kinet Catal Lett. 2003;79:93–9.
29. Cutrufello MG, Ferino I, Rombi E, Solinas V, Colón G, Navío JA. Acid-base properties of a Ceria-Lanthana catalytic system. J Therm Anal Calorim. 2003;72:223–9.
30. Cutrufello MG, Ferino I, Monaci R, Rombi E, Solinas S. Acid-base properties of zirconium, cerium and lanthanum oxides by calorimetric and catalytic investigation. Top Catal. 2002;19:225–40.
31. Casenave S, Martinez H, Guimon C, Auroux A, Hulea V, Cordoneanu A, Dumitriu E. Acid-base properties of Mg–Ni–Al mixed oxides using LDH as precursors. Thermochim Acta. 2001;379:85–93.
32. Casenave S, Martinez H, Guimon C, Auroux A, Hulea V, Dumitriu E. Acid and base properties of MgCuAl mixed oxides. J Therm Anal Calorim. 2003;72:191–8.
33. Xu M, Gines MJL, Hilmen AM, Stephens BL, Iglesia E. Isobutanol and methanol synthesis on copper catalysts supported on modified magnesium oxide. J Catal. 1997;171:130–47.
34. Han Y, Shen J, Chen Y. Microkinetic analysis of isopropanol dehydrogenation over Cu/SiO_2 catalyst. Appl Catal A. 2001;205:79–84.
35. David O, Meloni D, Monaci R, Solinas V, Ungureanu A, Chirieac A, Dumitriu E. The catalytic dehydrogenation of trans-cinnamaldehyde over mixed oxides derived from quaternary hydrotalcite-like precursors. Iasi: Faculty of chemical Engineering ZFIC; 2008. pp. 217–26.
36. Sing KSW, Everett DH, Haul RAW, Moscow L, Pierotti RA, Rouquerol J, Siemieniewska T. Reporting physisorption data for gas/solid systems—with special reference to the determination of surface area and porosity. Pure Appl Chem. 1985;57:603–19.
37. Ruthven DM. Principles of adsorption & adsorption processes. New York: Wiley; 1984.
38. Reid RC, Pransuitz JM, Sherwood TK. The properties of gases and liquids. 3rd ed. vol 27. New York: Mc Graw-Hill; 1977. p. 403–35.
39. Sedlácek J, Kraus M. Quantum chemical calculations on the catalytic dehydration of 2-propanol. React Kinet Catal Lett. 1975;2:57–63.
40. Nondek L, Sedlácek J. Mechanism of dehydrogenation of secondary alcohols on chromia. J Catal. 1975;40:34–9.